J. Fluid Mech. (2008), *vol.* 598, *pp.* 429–450. © 2008 Cambridge University Press
doi:10.1017/S0022112007000079 Printed in the United Kingdom

Evidence of higher-order effects in thermally driven rapid granular flows

C. M. HRENYA[1]†, J. E. GALVIN[1,2] AND R. D. WILDMAN[3]

[1]Department of Chemical and Biological Engineering, University of Colorado, Boulder, CO 80309-0424, USA

[2]United States Department of Energy National Energy Technology Laboratory (NETL), Morgantown, WV 26507-0880, USA

[3]Wolfson School of Mechanical and Manufacturing Engineering, Loughborough University, Loughborough, Leicestershire, LE11 3TU, UK

(Received 18 May 2007 and in revised form 21 November 2007)

Molecular dynamic (MD) simulations are used to probe the ability of Navier–Stokes-order theories to predict each of the constitutive quantities – heat flux, stress tensor and dissipation rate – associated with granular materials. The system under investigation is bounded by two opposite walls of set granular temperature and is characterized by zero mean flow. The comparisons between MD and theory provide evidence of higher-order effects in each of the constitutive quantities. Furthermore, the size of these effects is roughly one order of magnitude greater, on a percentage basis, for heat flux than it is for stress or dissipation rate. For the case of heat flux, these effects are attributed to super-Burnett-order contributions (third order in gradients) or greater, since Burnett-order contributions to the heat flux do not exist. Finally, for the system considered, these higher-order contributions to the heat flux outweigh the first-order contribution arising from a gradient in concentration (i.e. the Dufour effect)

1. Introduction

Rapid flows of solid particulates occur in a wide array of granular and multiphase systems. Examples include the motion of particulates in planetary rings, the top layer of pharmaceutical powders mixing in a tumbler, and high-velocity gas-fluidized beds as used in the gasification of coal and biomass, the synthesis of titania, etc. Continuum models based on an analogy with the kinetic theory of gases have been used widely over the last several decades to describe such flows (see review articles by Campbell 1990; Sundaresan 2000; Goldhirsch 2003; Curtis & van Wachem 2004; Goldhirsch, Noskowicz & Bar-Lev 2004; Wassgren & Curtis 2006). The accuracy of kinetic-theory-based models for granular flows has been tested using two general approaches. In the first approach, the governing equations are applied to a specific system along with appropriate initial and/or boundary conditions; the profiles of the predicted hydrodynamic profiles are then compared to those obtained via experiments or molecular dynamics (MD) simulations. In the second approach, fluxes and/or transport coefficients are extracted from MD simulations and compared to those predicted from kinetic-theory-based models. The latter approach, which is the focus of the current effort, allows for a more direct comparison since errors do not propagate from one quantity/expression (hydrodynamic variables, boundary conditions, etc.) to

† Author to whom correspondence should be addressed: hrenya@colorado.edu

another (stress, heat flux, etc.). Nonetheless, several subtleties arise which make such a comparison non-trivial.

The main challenge associated with the extraction of transport coefficients from MD simulations or experiments is the need to know the form of the flux law *a priori*. A specific example is the first (Navier–Stokes) order approximation of the heat flux $\boldsymbol{q}$, which takes the form of Fourier's law ($\boldsymbol{q} = -k\nabla T$) according to some granular theories (Jenkins 1998), and includes the Dufour contribution ($\boldsymbol{q} = -k\nabla T - \mu\nabla n$) in others (Brey *et al.* 1998; Sela & Goldhirsch 1998; Garzó & Dufty; 1999), where k is the thermal conductivity, T is the granular temperature, μ is the Dufour coefficient, and n is the number density of particles. Given that fluxes (heat flux, momentum flux, etc.) can be measured in MD simulations, but not necessarily (or easily) the separate contributions to these fluxes or their functional dependence on the hydrodynamic fields (n, T), the calculated value of the transport coefficient depends on the assumed form of the flux law. A further complication is encountered when the Dufour contribution is included; namely, the number of unknown variables in the flux equation is two (k and μ). Various approaches have been taken to address these issues. Shattuck *et al.* (1999) assume Fourier's law holds in order to extract k from their MD simulations, which is then compared to kinetic-theory-based predictions. Herbst, Müller & Zippelius (2005) instead assume that both k and μ are constant over a domain in which both n and T vary, which thereby allows them to perform a best-fit of both the transport coefficients over various sets of simulation data. A more rigorous approach is taken by Soto, Mareschal & Risso (1999), who extract μ from locations in the domain where $\nabla T = 0$ and $\nabla n \neq 0$; at such points, the flux law reduces to $\boldsymbol{q} = -\mu\nabla n$ and thus only one unknown (μ) remains. Unfortunately, our own simulations (unpublished) indicate that such an approach is not robust for the system they examined since the location at which $\nabla T = 0$ often, though not always, coincides with the location at which $\nabla n = 0$, which thereby precludes the isolated extraction of μ.

Furthermore, previous studies have indicated that the form of the heat flux law used to obtain kinetic-theory-based predictions of various systems impacts even the qualitative nature of the resulting profiles. More specifically, when solving the boundary-value problem for a vibro-fluidized bed, the use of Fourier's law results in a monotonic decrease of temperature with an increase in bed height (Martin, Huntley & Wildman 2006). On the other hand, when the flux law which includes the ∇n driving force is used, a local minimum in granular temperature is observed at low bed heights (Brey, Ruiz-Montero & Moreno 2001; Martin, *et al.* 2006). Unfortunately, existing experimental data cannot be used to distinguish the correct behaviour because of the presence of the Knudsen layer at the open end of the system (Martin *et al.* 2006).

In an attempt to build on these previous efforts and gain a better understanding of the heat flux law and in particular the role of the Dufour contribution, MD simulations were performed for a simple bounded conduction system. In particular, the system under consideration is characterized by zero mean flow and opposing walls of two specified temperatures, which is a natural choice for investigations on heat flux. The constitutive quantities under examination include the heat flux, the stress tensor, and the dissipation rate of granular energy. A comparison of MD values and theoretical predictions of these quantities reveal that higher-order effects (i.e. beyond first-order in spatial gradients) play an important role. For the specific case of heat flux, these effects are at least super-Burnett-order (third-order in spatial gradients), and are significantly larger in magnitude than corrections provided by the Dufour contribution.

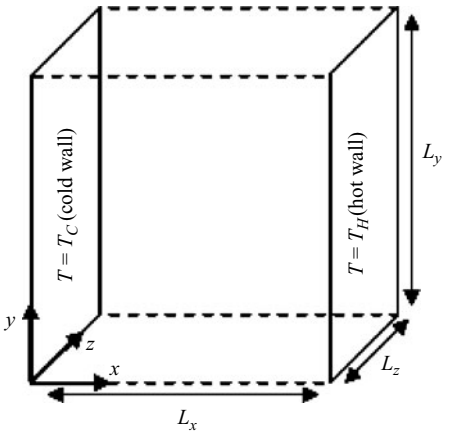

FIGURE 1. Schematic of bounded conduction system.

2. Molecular dynamics simulations: computational algorithm

2.1. *Bounded conduction*

Three-dimensional molecular dynamics (MD) simulations of identical spheres are carried out. The particles are treated as inelastic frictionless spheres and particle collisions are assumed to be binary and instantaneous. The system is bounded on the left and right by motionless walls of constant, but not necessarily equal, granular temperature (see figure 1). The remaining four sides (top, bottom, front and back) are standard periodic boundaries. Since no body forces are present, the system is characterized by zero mean flow. The present simulation will be briefly discussed; a more detailed description is contained elsewhere (Dahl & Hrenya 2004; Galvin *et al.* 2005, 2007).

The simulation domain is bounded on the left- and right-hand side by walls of constant set temperature (T_{set}) using a method for thermal walls presented by Cercignani (1987) and Pöschel & Schwager (2005). The post-collisional components of particle velocity parallel to the wall (i.e. in the y and z directions) are determined following the Box–Muller method for generating two tangential Gaussian distributions (Press *et al.* 1992):

$$c_{post,y} = \sqrt{-\frac{2T_{set}}{m_i}\ln(z_1)}\cos(2\pi z_2), \tag{1}$$

$$c_{post,z} = \sqrt{-\frac{2T_{set}}{m_i}\ln(z_3)}\sin(2\pi z_4), \tag{2}$$

where z_1–z_4 are random numbers uniformly distributed in the interval [0, 1]. The post-collisional component of particle velocity normal to the wall (in the x direction) is given by

$$c_{post,x} = \sqrt{-\frac{2T_{set}}{m_i}\ln(z_5)}, \tag{3}$$

where z_5 is a random number again uniformly distributed in the interval [0, 1]. The sign of this component is determined by reversing the sign (+ or −) of the pre-collisional component of particle velocity normal to the wall. As previously mentioned, the four remaining boundaries are standard periodic boundaries. Thus, a

particle crossing through one of these boundaries is returned through the opposing boundary with the same velocity and relative position.

The simulation proceeds in time based on a hard-particle/overlap algorithm (Hopkins & Louge 1991). For further details on particle initialization and the particle advancement algorithm, see Dahl & Hrenya (2004).

The simulation input parameters include the following: the length of the simulation domain in the x, y and z directions (L_x, L_y and L_z), the particle diameter (d),the particle mass (m), the average solids volume fraction in the (entire) system ($\bar{\nu}$), the coefficient of restitution (e), and the set values of the wall temperature located at $x/L_x = 0$ (T_C) and $x/L_x = 1$ (T_H). The dimensionless parameters characterizing the system are $\bar{\nu}$, e, T_H/T_C, L_x/d, L_y/L_x and L_z/L_x. In the present effort, L_x/d is set at a value of 35 to ensure that each simulation is described by a global reciprocal Knudsen number greater than 5 (i.e. $1/Kn > 5$), where the 'global' Knudsen number is defined as $Kn = \bar{\lambda}/L_x$and $\bar{\lambda} = d/(6\bar{\nu})$ is the spatially averaged mean free path. Accordingly, the total number of particles (N) in a given simulation will range from 4000 to 12000 depending on the values of the other dimensionless quantities ($\bar{\nu}$, L_y/L_x, L_z/L_x). In the present simulations the periodic domain lengths are set equal ($L_y = L_z$) with a value of $L_y/L_x = L_z/L_x = 1$; these values of the periodic domain lengths were found to be large enough that the collected data are not sensitive to further increases in these quantities. Consequently, the simulation domain is cubic ($L_x = L_y = L_z$) and the characteristic dimension is here in after referred to as L. The remaining parameter space under investigation includes the temperature ratio (T_H/T_C) with set values of 1, 2 and 15, $\bar{\nu} = 0.025 - 0.15$ ($Kn = 1.9 \times 10^{-1} - 3.2 \times 10^{-2}$) and $e = 0.8$ – 1. For convenience, the dimensional quantities m and L_x are set equal to 1.

The outputs from the simulation include lateral profiles of solids volume fraction (ν), granular temperature (T), heat flux ($\boldsymbol{q}$), stress tensor ($\boldsymbol{\sigma}$), and the dissipation rate of granular energy (γ). The granular temperature is defined as $T = 1/3\langle C^2 \rangle$ where $\boldsymbol{C}$ is the fluctuating velocity. Note that several output quantities (T, $\boldsymbol{q}$, $\boldsymbol{\sigma}$, γ) depend on the fluctuating velocity $\boldsymbol{C}$, which is defined relative to a local mass-average velocity. Since a zero local velocity is assumed in all calculations (as described in § 4, this assumption of no collective motion, or no clustering, does not impact on the results), the instantaneous particle velocity ($\boldsymbol{c}$) is equal to the fluctuating particle velocity and so the two may be used interchangeably. For further details on data collection, the reader is referred to Dahl & Hrenya (2004) and Galvin, Hrenya & Wildman (2007).

To determine the spatial variation in the output quantities the domain is divided into thin rectangular boxes aligned parallel to the walls of set temperature. The current simulations include 30 data collection strips so that the width of each data collection strip (Δx) is slightly wider than a particle diameter. The collected data do not change meaningfully with further resolution in the strip width.

For each strip, the hydrodynamic variables (ν, T) and the constitutive quantities ($\boldsymbol{q}$, $\boldsymbol{\sigma}$, γ) are reported. Only the portion of the particle volume that resides within a given data collection strip is included in determining the solids volume fraction of that strip. The granular temperature of each strip is determined by including only the granular temperature of particles whose centres reside within the data collection strip at the instant of measurement. Note that if both quantities are collected according to the former method (distribution of quantity based on volume fraction of particle residing in a given strip), the results are essentially identical to those presented below.

The total heat flux ($\boldsymbol{q}$) is comprised of two parts: a kinetic component ($\boldsymbol{q}_k$) and a collisional component ($\boldsymbol{q}_c$). Following the methods used by Herbst *et al.* (2005), the

kinetic contribution of the heat flux is determined using

$$q_{k,a,strip} = \frac{1}{V_{strip}} \sum_{i=1}^{n_{strip}} \tfrac{1}{2} m C_{strip}^2 C_{a,strip}. \tag{4}$$

In this equation, $C_{a,strip}$ is the fluctuating velocity of particle i in the a direction (where a can be x, y or z) in the specified strip, $C_{strip}^2 = \boldsymbol{C}_{strip} \cdot \boldsymbol{C}_{strip}$, V_{strip} is the volume of the strip ($V_{strip} = L_z L_y \Delta x$) and n_{strip} is the number of particles whose centres reside within the data collection strip. If a different, reasonable criterion is used, such as a distribution of flux according to volume fraction of particles residing in a strip, the resulting stress profile is found to be essentially identical. (This finding is also true for all remaining constitutive quantities discussed below, including both kinetic and collisional components.) Similarly, the collisional component of the heat flux is found by

$$q_{c,a,strip} = \frac{1}{2 V_{strip} \Delta t} \sum_{coll_{strip}} (\Delta E_1 - \Delta E_2) D k_a. \tag{5}$$

In this equation, Δt is the elapsed time since data collection was initiated, D is the distance between the particle centres, k_a is the a component of the unit vector pointing from the centre of particle 1 toward the centre of particle 2 ($a = x$, y, or z), ΔE_1 is the change in energy of particle 1 owing to a collision with particle 2, and ΔE_2 is the change in energy of particle 2 owing to a collision with particle 1. For a given particle, the quantity ΔE is defined as

$$\Delta E = \tfrac{1}{2} m \left(C_{post}^2 - C_{pre}^2 \right), \tag{6}$$

where the mass and fluctuation velocity are those quantities associated with the given particle. The collisional heat flux (equation (5)) is found by summing only the heat flux of particles whose centres reside within the data collection strip during the collision (summation over $coll_{strip}$). In the event that the centres of the two colliding particles lie in different strips, the collisional heat flux is divided equally between the adjacent data collection strips in which the particle centres reside.

The stress tensor also consists of a kinetic and a collisional contribution. The kinetic stress components ($\sigma_{k,ab}$) are calculated based on the equations used by Campbell & Gong (1986) applied to each collection strip:

$$\sigma_{k,ab,strip} = \frac{1}{V_{strip}} \sum_{i=1}^{n_{strip}} m C_{a,strip} C_{b,strip}. \tag{7}$$

In this equation, $C_{b,strip}$ is the fluctuating velocity of particle i in that strip in the b direction (where b can be x, y or z). The collisional stress components (also based on equations of Campbell & Gong 1986) are calculated as

$$\sigma_{c,ab,strip} = \frac{1}{V_{strip} \Delta t} \sum_{coll_{strip}} J_a D k_b, \tag{8}$$

$$\boldsymbol{J} = m_1 (\boldsymbol{C}_{1,pre} - \boldsymbol{C}_{1,post}), \tag{9}$$

where J_a is the a component of momentum impulse ($\boldsymbol{J}$) applied during the collision, k_b is the b component of the unit vector pointing from the centre of particle 1 toward the centre of particle 2 ($a,b = x$, y, or z), and D is the distance between the particles centres. In the impulse calculation, $\boldsymbol{C}_{1,post}$ is the post-collisional (random) particle velocity of particle 1, $\boldsymbol{C}_{1,pre}$ is the pre-collisional (random) particle velocity

of particle 1, and m_1 is the mass of particle 1. In this system, $D = d$ and $m_1 = m$. Similar to the collisional heat flux, the collisional stress within each data collection strip is found by including only the collisional stress of colliding particles whose centres reside within the data collection strip during the collision. In the event that the centres of the two colliding particles lie in different strips, the collisional stress is then divided equally between the adjacent data collection strips in which the particle centres reside.

The granular energy dissipation rate per unit volume (γ) is a measure of the change of energy resulting from a binary collision. Following Herbst *et al.* (2005), the energy dissipation rate is defined by

$$\gamma_{strip} = \frac{1}{V_{strip}\Delta t} \sum_{coll_{strip}} (\Delta E_1 + \Delta E_2), \tag{10}$$

where the terms are the same as those defined previously.

Unless otherwise specified, the data collection phase of each simulation comprises 50 000 collisions per particle during which 1 000 000 evenly spaced instantaneous measurements of solids volume fraction, granular temperature and the kinetic components of the heat flux and stress tensor are made. The collisional components of the constitutive quantities are evaluated as a summation over all collisions during the data collection portion of the simulation. The average of these measurements is calculated and reported at the end of the simulation. Measurements corresponding to the strips adjacent to the bounding walls are not reported owing to volume exclusion effects caused by the solid boundary. For details, see Galvin *et al.* (2007).

2.2. *Homogeneous cooling system*

As discussed in § 4, a number of simulations were also run for a homogeneous cooling system (HCS), in which the only modification to the bounded system described above is that all six faces of the cubic domain are periodic. Thus, the system is homogenous in the spatial domain. (As detailed in § 4, all data obtained from MD simulations was collected from a non-clustered state.) Furthermore, since no energy source exists, the system 'cools' with time (T decreases) for all $e < 1$. It is well known, and confirmed by the current MD simulations, that $\mathrm{d}T/\mathrm{d}t$ (which equals $-\gamma/n$ based on the governing equation for HCS) also varies with time, which complicates the collection of γ. Specifically, using (10) to find γ presents several challenges: (i) at small Δt, γ is noisy (T decreases monotonically with t, but its gradient is noisy) and (ii) at higher Δt, γ is found to depend on the size of the averaging region. These obstacles can be overcome, however, by considering the behaviour predicted by kinetic-theory-based models, namely $\mathrm{d}T/\mathrm{d}t \propto T^{3/2}$, which can be integrated to show that $\ln(T)$ *vs.* $\ln(t)$ is linear with a slope of $m = -2$, as is consistent with Haff's law (Haff 1983). Following from this relationship, $\mathrm{d}\ln(T)/\mathrm{d}\ln(t) = m$, which can be rearranged to give

$$\frac{\mathrm{d}T}{\mathrm{d}t} = m\frac{T}{t}. \tag{11}$$

In this manner, $\mathrm{d}T/\mathrm{d}t$ (and thus γ) can be determined using the value of hydrodynamic variable T from a single time point t, rather than having to evaluate the derivative of T at that time point. The MD simulations confirm that $\ln(T)$ *vs.* $\ln(t)$ becomes linear after roughly 15 collisions per particle, with a slope of approximately -2.

A further simplification can be made by considering the predicted dependency of γ on T. In particular, kinetic-theory-based models indicate that $\gamma \propto T^{3/2}$. Thus, although $\mathrm{d}T/\mathrm{d}t = -\gamma/n$ varies with time, $(\mathrm{d}T/\mathrm{d}t)/T^{3/2} = -\gamma/nT^{3/2}) = \gamma^*/n$ remains constant (since n and all other properties impacting γ are constant in the HCS), where γ^*

$(=\gamma/T^{3/2})$ is the dissipation rate divided by its known temperature dependency. This (long-time) constant behaviour is again confirmed by MD simulations. (In other words, the MD values of γ^* at short times depend on initial particle velocities (temperature) and/or positions, though the longer-time values are constant and independent of initial conditions.) Data are collected using a series of averaging periods with a duration of 25 collisions per particle, during which 1000 measurements of T and t are recorded. For each period, the best-fit slope of $\ln(T)$ *vs.* $\ln(t)$ is determined. If the slope is within 5% of the expected value of -2, the corresponding value of $\mathrm{d}T/\mathrm{d}t$ is determined for each of the 1000 time points using (11), and then non-dimensionalized via division by $T^{3/2}$. Based on the 1000 values of $\mathrm{d}T/\mathrm{d}t$, an average value of γ^* is then calculated for the given period. A minimum of three periods for the collection of γ^* is used. Once the cumulative average of γ^* over these periods differs by less than 1%, the simulation is stopped and the cumulative average of γ^* is recorded. All simulations were run with 100 particles in an effort to preclude the onset of clustering, as detailed in §4. The only exception made to this collection methodology is for $\bar{\nu}=0.5$ and $e=0.95$, in which the collection period is defined as 100 collisions per particle since T is noisier at low $\bar{\nu}$ and high e.

3. Theoretical predictions

In the following section, the constitutive quantities obtained from MD simulations are compared to predictions obtained from continuum theories for rapid granular flows. Specifically, the kinetic-theory-based predictions of Jenkins (1998), Sela & Goldhirsch (1998) and Garzó & Dufty (1999) are considered. In this effort, the theoretical predictions for the constitutive quantities ($\boldsymbol{q}$, γ and $\boldsymbol{\sigma}$) are obtained using the MD simulation profiles in ν and T as inputs to the theory. As a result, possible errors in the predictions of the hydrodynamic variables (ν and T, as obtained from solution of the boundary-value problem) are prevented from propagating to the predictions of the constitutive quantities.

All of the theories target uniform inelastic frictionless spheres engaging in binary collisions, which is identical to the treatment used in the MD simulations. The theories of Jenkins (1998) and Garzó and Dufty (1999) are both of Navier–Stokes-order, though a key difference exists in the derivation process. In particular, the theory of Jenkins (1998) is based on a nearly elastic assumption while the theory of Garzó & Dufty (1999) is based on an expansion about low Knudsen numbers, in which no restriction on the level of dissipation is made. Consequently, the resulting constitutive relations will have different dependencies on the hydrodynamic variables. These expressions for the constitutive quantities, as applied to the bounded conduction system, are summarized in table 1.

Unlike the theories of Jenkins (1998) and Garzó & Dufty (1999), the work of Sela & Goldhirsch (1998) is of Burnett order, though it is restricted to both the dilute and nearly elastic limits. The Burnett-order corrections (second-order in gradients) derived by Sela & Goldhirsch (1998) are contained in table 2 for the case of bounded conduction. The superscript B refers to terms of Burnett order. It is worth noting that Brey *et al.* (1998) have also derived Burnett-order corrections to the dissipation rate for dilute systems, without any restriction on the level of inelasticity. Specifically, explicit coefficients for $\nabla^2 T$ and $\nabla^2 n$ are given, though explicit expressions for the coefficients of $(\nabla T)^2$, $(\nabla n)^2$ and $\nabla T \cdot \nabla n$ are not included. Because all five of these Burnett-order gradients are non-zero in the bounded conduction problem examined here, a direct comparison with this theory is not carried out.

Jenkins (1998)

Heat flux

$$q_x = -\left\{\frac{75}{64}\frac{m}{d^2\sqrt{\pi}}\sqrt{T}\left[\frac{1}{g_0}+\frac{24}{5}\nu+\frac{144}{25}\left(1+\frac{32}{9\pi}\right)\nu^2 g_0\right]\right\}\frac{\mathrm{d}T}{\mathrm{d}x}$$

Dissipation rate of granular energy

$$\gamma = \frac{24\nu g_0}{d\sqrt{\pi}}(1-e)\,mnT^{3/2}$$

Pressure

$$P = \frac{6\nu}{\pi d^3}mT\,[1+4\nu g_0]$$

Garzó & Dufty (1999)

Heat flux

$$q_x = -\left\{\frac{75}{64}\frac{m}{d^2\sqrt{\pi}}\sqrt{T}\left[k_k^*\left(1+\frac{6}{5}\nu g_0(1+e)\right)+\frac{256\nu^2}{25\pi}g_0(1+e)\left(1+\frac{7}{32}c^*\right)\right]\right\}\frac{\mathrm{d}T}{\mathrm{d}x}$$
$$-\left\{\frac{25}{128}\frac{md\sqrt{\pi}T^{3/2}}{\nu}\left[\mu_k^*\left(1+\frac{6}{5}\nu g_0(1+e)\right)\right]\right\}\frac{\mathrm{d}n}{\mathrm{d}x}$$

Dissipation rate of granular energy

$$\gamma = \frac{12\nu g_0}{d\sqrt{\pi}}\left(1-e^2\right)\left(1+\frac{3}{32}c^*\right)mnT^{3/2}$$

Pressure

$$P = \frac{6\nu}{\pi d^3}mT\,[1+2\nu(1+e)\,g_0]$$

Additional quantities

$$k_k^* = \frac{2}{3}\left(\nu_k^*-2\varsigma^{(0)*}\right)^{-1}\left\{1+\frac{1}{2}\left(1+p^*\right)c^*+\frac{6}{10}\nu g_0(1+e)^2\left[2e-1+\left(\frac{1}{2}(1+e)-\frac{5}{3(1+e)}\right)c^*\right]\right\}$$

$$\nu_k^* = \frac{1}{3}(1+e)\,g_0\left[1+\frac{33}{16}(1-e)+\frac{19-3e}{1024}c^*\right]$$

$$\varsigma^{(0)*} = \frac{5}{12}g_0\left(1-e^2\right)\left(1+\frac{3}{32}c^*\right)$$

$$p^* = 1+2\nu(1+e)\,g_0$$

$$c^* = 32(1-e)\left(1-2e^2\right)\left[81-17e+30e^2(1-e)\right]^{-1}$$

$$\mu_k^* = 2\left(2\nu_k^*-3\varsigma^{(0)*}\right)^{-1}\left\{\left(1+n\frac{\partial \ln g_0}{\partial n}\right)\varsigma^{(0)*}k_k^*+\frac{p^*}{3}\left(1+n\frac{\partial \ln p^*}{\partial n}\right)c^*\right.$$
$$\left.-\frac{12}{15}\nu g_0\left(1+\frac{1}{2}n\frac{\partial \ln g_0}{\partial n}\right)(1+e)\left[e(1-e)+\frac{1}{4}\left(\frac{4}{3}+e(1-e)\right)c^*\right]\right\}$$

Carnahan & Starling (1969)

Radial distribution function

$$g_0 = \frac{2-\nu}{2(1-\nu)^3}$$

TABLE 1. Navier–Stokes order constitutive relations for bounded conduction system.

4. Results and discussion

Molecular-dynamics (MD) simulations of the bounded conduction system (figure 1) were carried out over a range of parameters, $\bar{\nu} = 0.025-0.15$, $e = 0.8-0.99$, and $T_H/T_C = 1-14$. The results presented in this section are representative of those obtained throughout the parameter space. Typical profiles of the mean flow fields are given in figure 2 for a system with $\bar{\nu} = 0.05$, $e = 0.8$ and $T_H/T_C = 1$. Because of the dissipative (inelastic) nature of particle-particle collisions, the granular temperature is at a minimum at the domain centre (figure 2*b*), with the left-hand and right-hand boundaries serving as a source of granular energy. As expected from the governing

Sela & Goldhirsch (1998)

Heat flux

$$q_x^B = 0$$

Dissipation rate of granular energy

$$\gamma^B = 0.2444\frac{\varepsilon\ell}{\theta^{1/2}}\left(\frac{d\theta}{dx}\right)^2 - 0.0834\frac{\varepsilon\ell}{n\theta^{1/2}}\left(\frac{\mathrm{d}(n\theta)}{\mathrm{d}x}\right)\left(\frac{\mathrm{d}\theta}{\mathrm{d}x}\right) + 0.0692\varepsilon\ell\theta^{1/2}\left(\frac{\mathrm{d}^2\theta}{\mathrm{d}x^2}\right)$$

Stress tensor

$$\sigma_{xx}^B = -0.6422n\ell^2\left[\frac{1}{3}\left\{\frac{1}{n}\left(\frac{\mathrm{d}^2(n\theta)}{\mathrm{d}x^2}\right) - \frac{1}{n^2}\left(\frac{\mathrm{d}n}{\mathrm{d}x}\right)\left(\frac{\mathrm{d}(n\theta)}{\mathrm{d}x}\right)\right\}\right] + 0.2552n\ell^2\left(\frac{\mathrm{d}^2\theta}{\mathrm{d}x^2}\right)$$
$$+ 0.0719\frac{\ell^2}{\theta}\left(\frac{\mathrm{d}(n\theta)}{\mathrm{d}x}\right)\left(\frac{\mathrm{d}\theta}{dx}\right) + 0.0231\frac{n\ell^2}{\theta}\left(\frac{\mathrm{d}\theta}{\mathrm{d}x}\right)^2$$

$$\sigma_{yy}^B = \sigma_{zz}^B = 0$$

Additional quantities

$$\theta = 3T$$
$$\varepsilon = 1 - e^2$$
$$\ell = \frac{1}{\pi n d^2}$$

TABLE 2. Burnett–order corrections to constitutive relations for bounded conduction system.

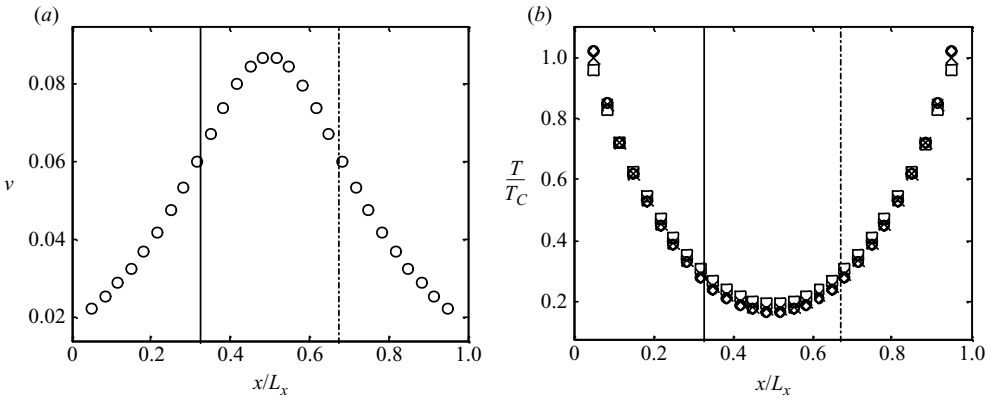

FIGURE 2. MD profiles of flow field variables (*a*) solids volume fraction, (*b*) non-dimensional granular temperature. MD simulations for total temperature (cross), *y*-component (squares), *x*-component (circles) and *z*-component (diamonds). Reciprocal local Knudsen numbers of 2.5 evaluated from the cold, left (solid vertical line) and hot, right (dash-dot vertical line). Relevant parameters are $e = 0.8$, $\bar{\nu} = 0.05$, $T_H/T_C = 1$, $L/d = 35$.

equations for this system (Galvin *et al.* 2007), the solids concentration and granular energy are inversely related, thereby leading to a maximum value of packing fraction at the centre of the domain (figure 2*a*).

In figure 3, MD profiles for each of the constitutive quantities are displayed for the same set of system parameters considered in figure 2. As evident from figure 3*a*, granular energy is transported from the walls to the centre of the domain, i.e. the heat flux q_x is positive on the left-hand side of the domain and negative on the right-hand side. Furthermore, the heat flux is greatest in magnitude near the walls and zero at the centre of the domain since the flow-field gradients are zero at $x/L = 0.5$. Profiles of the normal stress components are contained in figure 3(*b*), in which σ_{xx} is seen to be constant across the domain while $\sigma_{yy} = \sigma_{zz}$ are seen to display a minimum in the centre. As pointed out by Herbst *et al.* (2004), this non-constant behaviour of σ_{yy} and

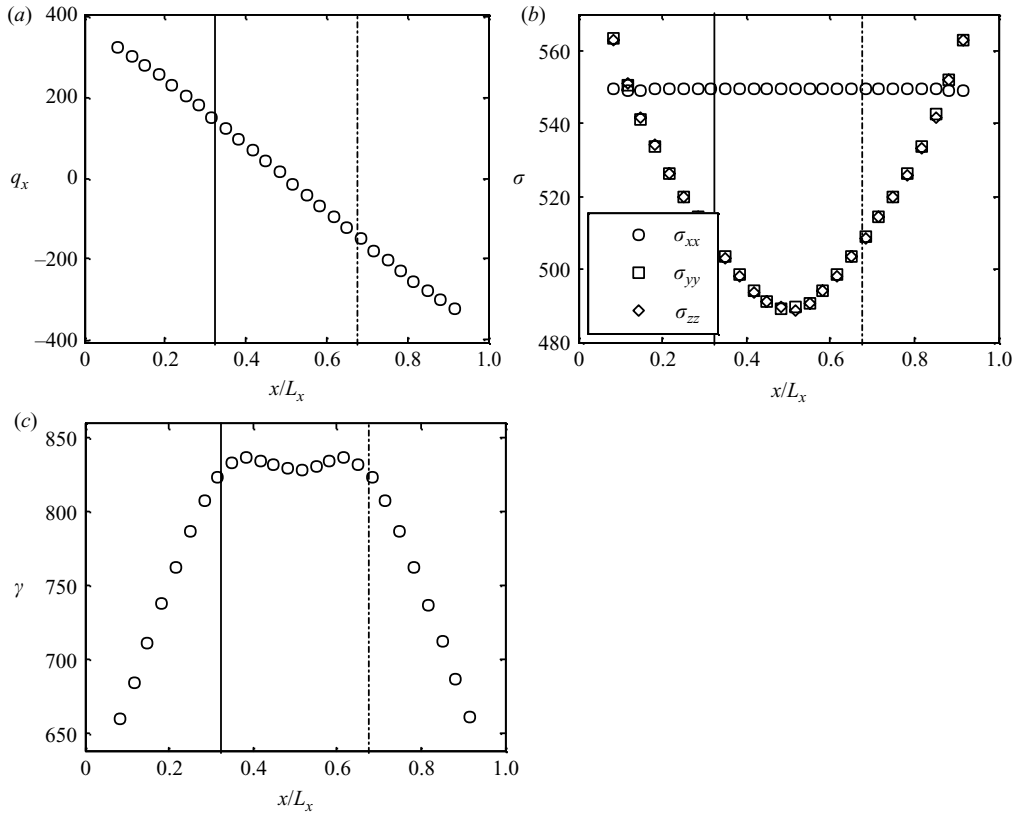

FIGURE 3. MD profiles of constitutive quantities (*a*) heat flux, (*b*) stress components, and (*c*) dissipation rate. MD simulations for xx-component of stress (circles), yy-component (squares) and zz-component (diamonds). Vertical lines are as in figure 2. Relevant parameters are $e = 0.8$, $\nu = 0.05$, $T_H/T_C = 1$, $L/d = 35$.

σ_{zz} is not contrary to the behaviour dictated by the Navier–Stokes-order equations. Namely, the only non-vanishing component of the momentum balance is the x-component, which reduces to $\mathrm{d}\sigma_{xx}/\mathrm{d}x = 0$ or $\sigma_{xx} =$ constant. Although the y- and z-components contain the terms $\partial\sigma_{yy}/\partial y$ and $\partial\sigma_{zz}/\partial z$, respectively, all $\partial/\partial y$ and $\partial/\partial z$ terms vanish in the current system owing to the periodic boundaries, so σ_{yy} and σ_{zz} are not necessarily restricted to constant values. Figure 3(*c*) demonstrates the behaviour of the dissipation rate, which displays its minimum values at the boundaries and a small local minimum in the middle of the domain. This minimum becomes more prominent at higher values of $\bar{\nu}$ and disappears for lower values of $\bar{\nu}$ (figures not shown).

To ensure that the results obtained from simulations are not subject to errors associated with insufficient averaging times, etc., high-accuracy simulations were performed. In particular, the MD values for the constitutive quantities were verified via a check of the governing equations, namely $\mathrm{d}\sigma_{xx}/\mathrm{d}x = 0$ (x-component of the momentum balance) and $0 = -\mathrm{d}q_x/\mathrm{d}x - \gamma$ (granular energy balance). The corresponding percentage errors obtained from MD, as displayed in figures 4(*a*) and 4(*b*), respectively, are calculated according to

$$\begin{pmatrix}\%\text{ error in } x\text{-component}\\ \text{of momentum balance}\end{pmatrix} = \frac{\sigma_{xx,MD} - \bar{\sigma}_{xx,MD}}{\bar{\sigma}_{xx,MD}} \times 100, \tag{12}$$

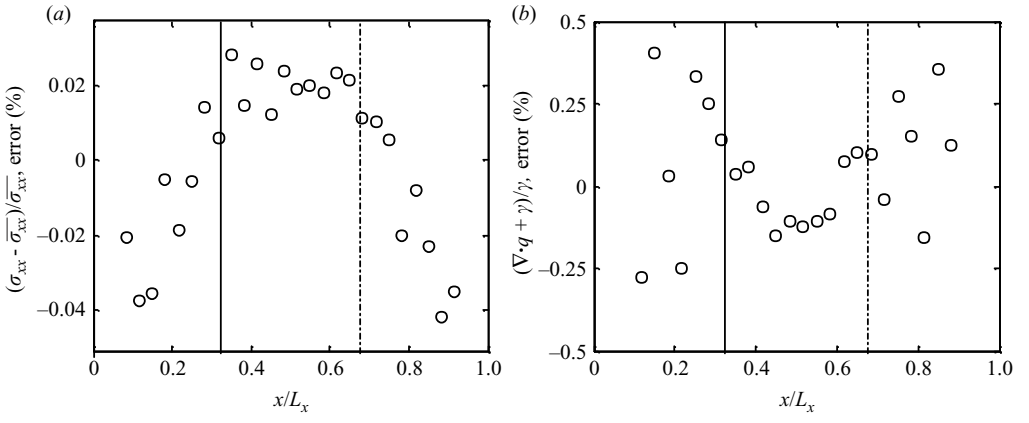

FIGURE 4. MD verification of constitutive quantities (*a*) percentage error in momentum balance and (*b*) percentage error in energy equation. MD simulations (circles). Vertical lines are as in figure 2. Relevant parameters are $e = 0.8$, $\bar{\nu} = 0.05$, $T_H/T_C = 1$, $L/d = 35$.

$$\begin{pmatrix}\%\text{ error in granular}\\ \text{energy balance}\end{pmatrix} = \frac{-\dfrac{\mathrm{d}q_{x,MD}}{\mathrm{d}x} - \gamma_{MD}}{\gamma_{MD}} \times 100, \tag{13}$$

where the overbar refers to the average value obtained across the simulation domain and the MD-subscript indicates values obtained from the MD simulations. As demonstrated by figure 4, the maximum error observed for either balance equation is less than 0.5%.

For the results presented below, two precautions are taken to make certain that the comparison between theory and simulations is as fair as possible. First, as mentioned above, MD values for the hydrodynamic variables (ν and T) are used as inputs to the theoretical predictions for the constitutive quantities (equations (4), (5), (7), (8) and (10)) as opposed to solving the corresponding BVP (boundary value problem). For the latter approach, any errors in the predicted profiles for ν and T would propagate to the theoretical evaluation of constitutive quantities. This situation is avoided by using the MD profiles as inputs. Secondly, attention is focused on the bulk interior, since comparisons are being made with continuum theories that incorporate particle–particle, but not particle–wall, collisions. More specifically, comparisons in the near-wall region are ignored since the transport coefficients in this Knudsen layer are impacted by the detailed nature of the wall (through particle–wall collisions) whereas the bulk interior is dictated by particle–particle collisions. The thickness of the Knudsen layer is thus expected to be of the order of a mean free path, since after travelling this distance from the wall, particles are likely to have engaged in a particle–particle collision. The identification and impact of the Knudsen layer for the system under consideration was explored in detail by Galvin *et al.* (2007). An example of these findings is given in figure 5, which include MD profiles of the granular temperature gradient (figure 5*a*) and heat flux (figure 5*b*). In molecular systems, a 'slip' or 'jump' in temperature characterizes the transition from the bulk interior to the Knudsen layer (Ferziger & Kaper 1972; Mackowski, Papadopoulos & Rosner 1999). In the granular systems considered here, such a jump may be evident from an abrupt change in the slope of the ∇T profile ($x/L_x \sim 0.7$ in figure 5*a*) but may also be too subtle for easy detection ($x/L_x \sim 0.2$ in figure 5*a*). A more robust method for identifying the width of the Knudsen layer is via an examination of the

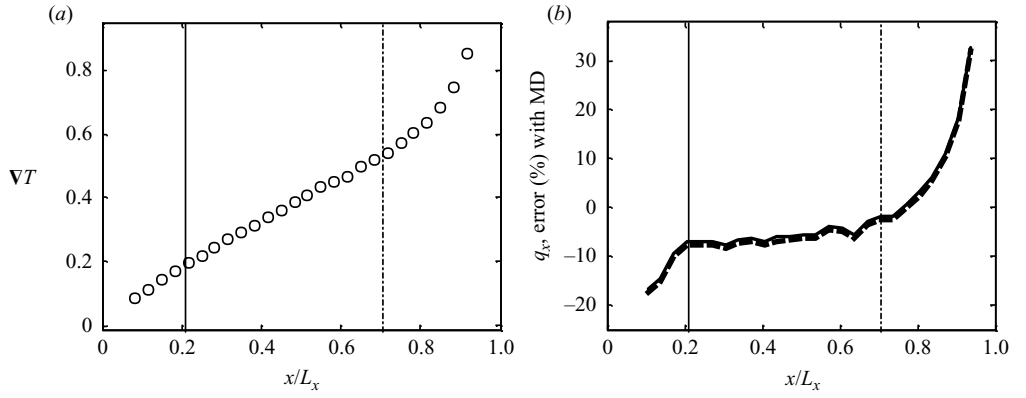

FIGURE 5. Identification of Knudsen boundary layers via (*a*) MD profiles of the temperature gradient and (*b*) the percentage error in heat flux between MD simulations and theoretical predictions. MD simulations (circles); Jenkins (1998) predictions (solid line); Garzó & Dufty (1999) predictions (thick dotted line). Vertical lines are as in figure 2. Relevant parameters are $e = 0.99$, $\bar{\nu} = 0.05$, $T_H/T_C = 2$, $L/d = 35$.

error between the theoretical heat flux with that obtained from MD (figure 5*b*). In the event that heat flux data are not available (as is true for experiments), an alternative method for identifying the Knudsen layer is via a reciprocal (local) Knudsen number,

$$\frac{1}{Kn_{wall}} = \frac{\ell_{wall}}{\lambda_{wall}} = \left(\frac{\ell}{\lambda}\right)_{wall}, \tag{14}$$

where ℓ_{wall} is the distance between a given wall and a point interior to the domain (e.g. the vertical line) and λ_{wall} is the mean free path defined in terms of the average solids fraction ($\bar{\nu}_{wall}$) between the wall and the distance ℓ_{wall} ($\lambda_{wall} = d/(6\bar{\nu}_{wall})$ for three-dimensional systems). For the systems under consideration here, a value of $(\ell/\lambda_{wall}) = 2.5$ was found to coincide with the bulk-to-Knudsen-layer transition predicted by the heat flux measurements; see figure 5(*b*) where these values for the left- and right-hand walls are demarcated by the solid and dashed vertical lines, respectively. Similar lines are contained in figures 2 to 6 and 8 to 10. For the remainder of this section, attention will be paid to the bulk interior (the region between the two vertical lines) in order to make the fairest possible comparison between the existing continuum theories and the MD data.

In figure 6, a comparison is made between the MD values for the dissipation rate (γ) and the theoretical predictions of Jenkins (1998) and Garzó & Dufty (1999). (Another set of predictions is also included, as will be discussed below.) The comparison is plotted as a percentage error, namely $100 \times (\text{theory} - \text{MD})/\text{MD}$, for the case of $\bar{\nu} = 0.05$, $T_H/T_C = 1$, and for two restitution coefficients, namely $e = 0.99$ (figure 6*a*) and $e = 0.8$ (figure 6*b*). Excellent agreement is observed at $e = 0.99$, with less than 1% error for both theories. At $e = 0.8$, the magnitude of the error in the bulk interior increases for both theories up to 5–10%. Furthermore, the maximum error (−10%) in the Garzó & Dufty (1999) theory over the bulk interior at $e = 0.8$ is greater than that (5%) of Jenkins (1998). The increase in error level with increasing dissipation is expected from the Jenkins (1998) theory since it is derived using a nearly elastic assumption. However, these trends are surprising for the Garzó & Dufty (1999) theory since it is derived without any restrictions on dissipation levels.

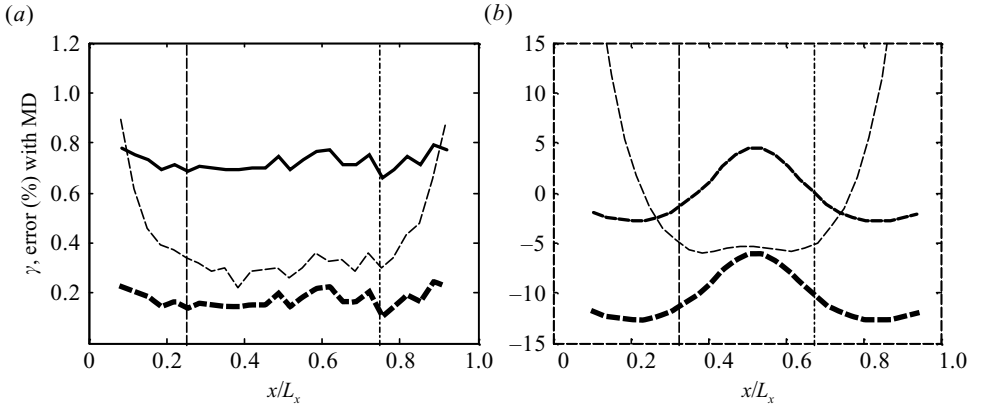

FIGURE 6. The percentage error in dissipation rate between MD simulations and theoretical predictions for two different inelasticities (*a*) $e = 0.99$ and (*b*) $e = 0.8$. Jenkins (1998) predictions (solid line); Garzó & Dufty (1999) predictions (thick dotted line); Garzó & Dufty with Sela & Goldhirsch corrections (thin dashed line). Vertical lines are as in figure 2. Remaining relevant parameters are $\bar{\nu} = 0.05$, $T_H/T_C = 1$, $L/d = 35$.

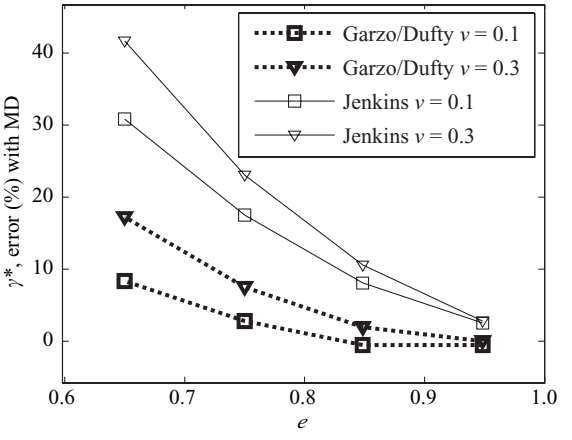

FIGURE 7. The percentage error in the modified dissipation rate ($\gamma^* = \gamma/T^{3/2}$) between MD simulations and theoretical predictions for a homogeneous cooling system. Jenkins (1998) predictions (thin solid line) for $\bar{\nu} = 0.1$ (squares) and $\bar{\nu} = 0.3$ (triangles). Garzó & Dufty (1999) predictions (thick dotted line) for $\bar{\nu} = 0.1$ (squares) and $\bar{\nu} = 0.3$ (triangles).

To gain further insight on the unexpected behaviour of the Garzó & Dufty (1999) theory at lower restitution coefficients, the homogeneous cooling system (HCS) is also examined. Unlike the bounded conduction problem, the HCS has periodic conditions on all six faces of the cubic domain. Thus, the boundaries do not provide an energy source, and the system cools with time. The resulting percentage error in the modified dissipation rate ($\gamma^* = \gamma/T^{3/2}$) between the MD simulations and the theories of Jenkins (1998) and Garzó & Dufty (1999) is presented in figure 7 as a function of e. Profiles are shown for both $\bar{\nu} = 0.1$ and 0.3. As expected (though contrary to figure 6), the Garzó & Dufty (1999) theory displays a significantly smaller error (this error may be due to inaccuracies associated with g_0) than that of Jenkins (1998) across the range of e and $\bar{\nu}$ examined. Two additional observations are noteworthy. First, in both figures 6 and 7, the Jenkins (1998) predictions are

higher than those of Garzó & Dufty (1999). Secondly, for the HCS (figure 7), the theory for Garzó & Dufty (1999) overpredicts the MD values, whereas the opposite is true for the bounded conduction problem (figure 6). Together, these observations imply a shift downward of predictions from both theories relative to MD values when switching from the HCS to the bounded conduction system.

To summarize the findings portrayed in figures 6 and 7, the HCS comparisons of dissipation rate are more consistent with the expectations for each theory than those of the bounded conduction problem. Namely, for the HCS, less error is obtained with the Garzó & Dufty (1999) predictions over the range of e examined since its derivation does not impose any restrictions on the dissipation level. One possible reason for the apparent inconsistency between the HCS and bounded conduction problem is the potential presence of clusters (transients in local particle concentration) in either system, as have been observed in MD simulations of the HCS (Goldhirsch & Zanetti 1993), simple shear flows (Hopkins & Louge 1991; Tan & Goldhirsch 1997; Liss & Glasser 2001; Lasinski, Curtis & Pekny 2004), and vibro-fluidized beds (Sunthar & Kumaran 2001). For the HCS system, the length scale required in order to preclude the clustering instability, as predicted by Brey *et al.* (2006), was used as a guide for the system size. Haff's law (Brilliantov & Pöschel 2004) was used as a further check; if Haff's law was violated, data collection was forced to cease and the simulation was halted. For the case of bounded conduction, the analysis of Galvin *et al.* (2005) indicates that clusters are not present over the range of parameters examined. Thus, the presence of clusters in both systems is intentionally avoided.

The remaining key difference between the HCS and the bounded conduction is related to the spatial gradients in the hydrodynamic variables. By definition, the (non-clustering) HCS is homogeneous and thus has zero spatial gradients throughout the domain, while the bounded conduction problem displays gradients in each of the hydrodynamic variables (figure 2) and constitutive quantities (figure 3). For this reason, the HCS provides an ideal system with which to compare Navier–Stokes-order dissipation rates,† which is consistent with the improved performance of the Garzó & Dufty (1999) theory over that of Jenkins (1998) for this system (figure 7). Thus, a possible explanation for the reversal of the relative performance of the two theories in the bounded conduction problem is the presence of higher-order (beyond Navier–Stokes-order) gradients which are not negligible. To test this idea, a third set of predictions is included in figure 6. In particular, the Burnett-order (second-order in gradients) corrections of Sela & Goldhirsch (1998) are added to the Navier–Stokes (first-order in gradients) predictions of Garzó & Dufty (1999). Two restrictions on the Sela & Goldhirsch (1998) theory are noteworthy. First, the theory was developed for flows in the nearly elastic limit. Thus, the qualitative nature of the correction should be examined more than the quantitative, particularly at higher dissipation levels. Secondly, the Sela & Goldhirsch (1998) theory is restricted to the dilute limit, unlike the theory of Garzó & Dufty (1999), which is why a combination of these theories is used.‡ (For example, the predicted collisional contribution to the pressure is ~4% of the total pressure for a solids fraction of only 0.01; this relative contribution increases

† In addition to γ, a term proportional to $\nabla\cdot\boldsymbol{U}$ also contributes to the first (Navier–Stokes)-order expression for the dissipation rate of Garzó & Dufty (1999). However, this term is zero for both the HCS and the bounded conduction problem and thus only the zeroth-order contribution, or γ, is relevant in this work.

‡ A cleaner approach is to instead run simulations in the dilute limit, and then compare with the dilute-limit theory. Such simulations, however, become computationally prohibitive in order to avoid a system composed entirely of a Knudsen layer. Specifically, since $L/\lambda = 6\nu\ L/d$, L/d must

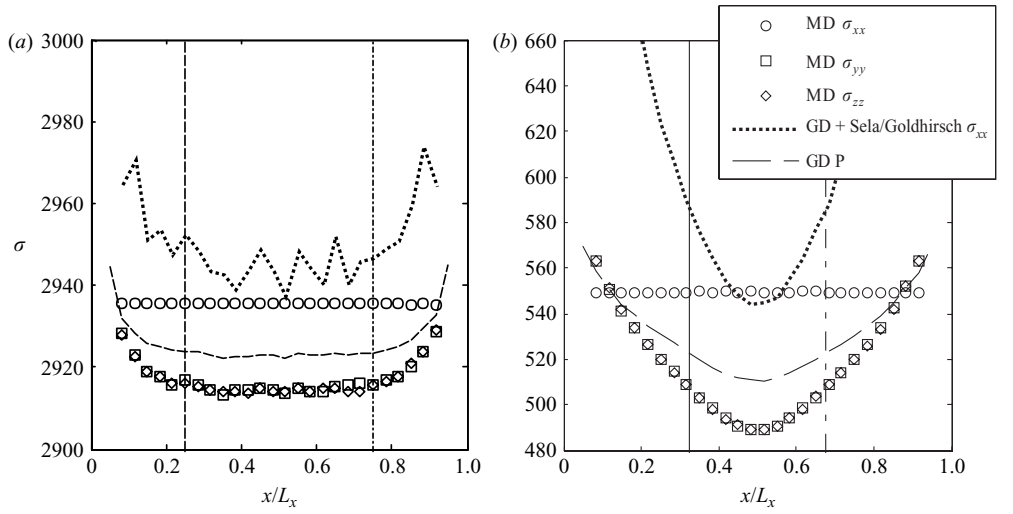

FIGURE 8. MD profiles and theoretical predictions of the stress components for two different inelasticities (*a*) $e = 0.99$ and (*b*) $e = 0.8$. MD simulations for xx-component of stress (circles), yy-component (squares), and zz-component (diamonds); Garzó & Dufty with Sela & Goldhirsch corrections of yy-component of stress (thin dashed line) and xx-component (thick dotted line). Vertical lines are as in figure 2. Relevant parameters are $\bar{\nu} = 0.05$, $T_H/T_C = 1$, $L/d = 35$.

with $\bar{\nu}$.) For the case of $e = 0.99$ (figure 6*a*), the Burnett-order corrections (i.e. the difference between the Garzó & Dufty 1999 predictions and the Garzó & Dufty 1999/Sela & Goldhirsch 1998) are on the order of the MD accuracy (figure 4). For $e = 0.8$, however, the Burnett-order corrections push the predictions of the Garzó & Dufty (1999) theory in the correct direction. Specifically, the error across the bulk interior ($0.3 < x/L_x < 0.7$) is roughly constant at -5%, whereas without the Burnett-order corrections the error reaches -10% at the boundaries of the bulk interior. This difference in the impact of Burnett-order terms at the two restitution coefficients can be explained in terms of the spatial gradients. In particular, at the limit of $e = 1$, all spatial gradients are equal to zero for the system under consideration. As the dissipation level increases, however, the magnitude of both first- and second-order gradients increases (figures not shown). Thus, Burnett-order effects are expected to become more important at lower e. Correspondingly, the reduction of error observed with the inclusion of Burnett-order corrections (figure 6*b*) is consistent with the presence of non-negligible higher-order effects in this system. Note that the identical Burnett-order correction could also be added to the Jenkins (1998) theory (since MD values are used as inputs to the correction), which would increase the magnitude of the resulting error. This increased error is not inconsistent with the previous conclusion on the role of Burnett-order effects, however. In particular, since the Jenkins (1998) theory is based on a nearly elastic assumption, the errors associated with higher inelasticities and Burnett-order effects cannot easily be decoupled, as is the case for the Garzó & Dufty (1999) theory which does not involve the nearly elastic assumption.

Further confirmation of the non-negligible role of higher-order effects is available from figure 8, in which the components of the stress tensor are illustrated for the case

be increased as ν is decreased in order to maintain a (minimum) value of L/λ. Because $N \propto (L/d)^3$, the corresponding computational expenses rise drastically.

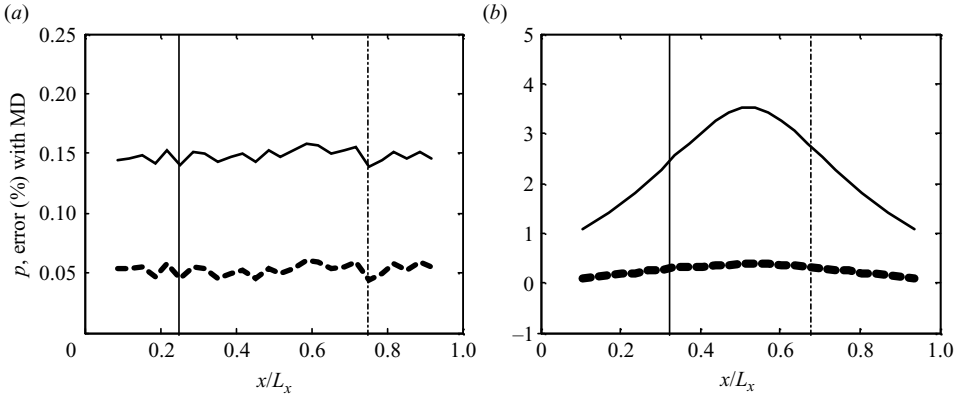

FIGURE 9. The percentage error in pressure between MD simulations and theoretical predictions for two different inelasticities (*a*) $e = 0.99$ and (*b*) $e = 0.8$. Jenkins (1998) predictions (thin solid line); Garzó & Dufty (1999) predictions (thick dotted line). Vertical lines are as in figure 2. Remaining relevant parameters are $\bar{\nu} = 0.05$, $T_H/T_C = 1$, $L/d = 35$.

of $\bar{\nu} = 0.05$, $T_H/T_C = 1$, and $e = 0.99$ (figure 8*a*) and $e = 0.8$ (figure 8*b*). Note that the MD values of σ_{xx} are constant across the domain, whereas σ_{yy} and σ_{zz} display minima at the centre of the domain. This behaviour is consistent with the momentum balance for this system. Namely, the x-component reduces to $\mathrm{d}\sigma_{xx}/\mathrm{d}x = 0$ ($\sigma_{xx} =$ constant), whereas the y- and z-components ($\partial\sigma_{xy}/\partial x = 0$ and $\partial\sigma_{xz}/\partial x = 0$, respectively) provide no further restrictions on the remaining normal (σ_{yy} and σ_{zz}) stress components (Herbst *et al.* 2004). However, this behaviour is not consistent with Navier–Stokes-order approximations. Such approximations reduce to $\mathrm{d}P/\mathrm{d}x = 0$ for this system, where $P = 1/3\ (\sigma_{xx} + \sigma_{yy} + \sigma_{zz})$. In particular, the MD results indicate that P is not constant across the domain, and thus the Navier–Stokes-order approximation is not upheld. Instead, the presence of anisotropy provides direct evidence of effects that are at least Burnett order, as was shown by Goldhirsch & Sela (1996). More specifically, although the boundaries employed here (equations (1)–(3)) impose a slight amount of anisotropy at the walls (see near-wall values of figures 8*a* and 8*b*), such effects are not expected to penetrate beyond the Knudsen layer since the particles will have engaged in a sufficient number of collisions before exiting this layer to effectively erase any boundary-induced anisotropy. This idea is corroborated by the qualitative shift in the nature of the anisotropy, namely $\sigma_{xx} < \sigma_{yy}\ (= \sigma_{zz})$ in the near-wall region, whereas the opposite is true in the bulk interior. Accordingly, the anisotropy in the bulk interior is attributed to higher-order gradients involving n and T. As further evidence of higher-order effects, the Burnett-order corrections of Sela & Goldhirsch (1998) are seen to push the predictions of the Navier–Stokes-order theory (Garzó & Dufty 1999) for σ_{xx} (i.e. $\sigma_{xx} = P$) in the direction of the MD data. (Note that according to the Sela & Goldhirsch (1998) theory, no Burnett-order corrections exist for σ_{yy} and σ_{zz} in this system, so only predictions for σ_{xx} and P are included in this plot.)

For the same set of parameters as used for figure 8, figure 9 presents the percentage error in the pressure obtained by MD and that predicted by the Navier–Stokes-order theories. For the nearly elastic case of $e = 0.99$ (figure 9*a*), the errors of both theories are less than 0.2%. For $e = 0.8$ (figure 9*b*), the error associated with the Jenkins (1998) theory increases to just over 3% at the domain centre, while the error associated with the Garzó & Dufty (1999) theory reaches a maximum of 0.3%.

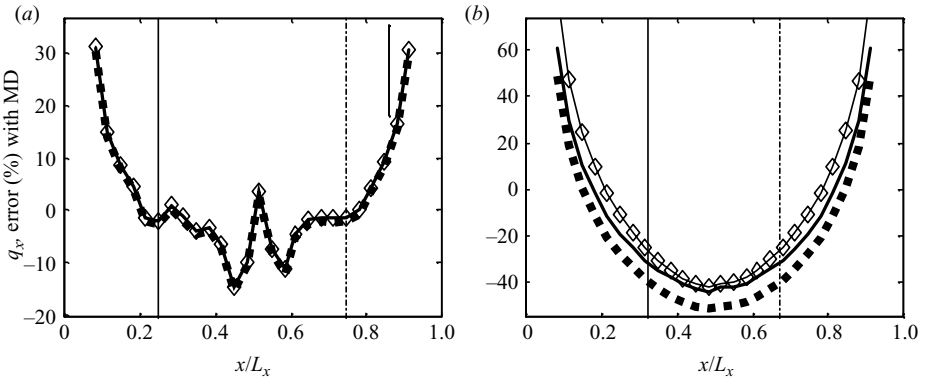

FIGURE 10. The percentage error in heat flux between MD simulations and theoretical predictions for two different inelasticities (*a*) $e = 0.99$ and (*b*) $e = 0.8$. Jenkins (1998) predictions (solid line); Garzó & Dufty (1999) predictions both excluding (thin dotted line with diamonds) and including (thick dotted line) gradient in number density term. Vertical lines are as in figure 2. Remaining relevant parameters are $\nu = 0.05$, $T_H/T_C = 1$, $L/d = 35$.

Comparisons involving the final constitutive quantity, heat flux, are depicted in figure 10 for the same conditions: $\bar{\nu} = 0.05$, $T_H/T_C = 1$, and $e = 0.99$ (figure 10*a*) and $e = 0.8$ (figure 10*b*). For the theories of both Jenkins (1998) and Garzó & Dufty (1999), the magnitude of the error in q_x for $e = 0.99$ is a few per cent in the domain interior relative to the MD data. At $e = 0.8$, however, the error associated with both Navier–Stokes-order theories increases in magnitude to nearly 40%. It is worth noting that this error is roughly one order of magnitude greater than that observed with the other constitutive quantities; see figures 6(*b*) and 9(*b*) for analogous comparisons of γ and P, respectively. Moreover, this error becomes even larger at higher concentrations; a system with $\bar{\nu} = 0.10$ and $e = 0.99$ results in an error of 5–10% in the bulk of the domain (figure not shown) compared to the relatively few per cent observed in figure 10(*a*). Although Burnett corrections were shown to provide an improvement for γ and P (figures 6*b* and 8*b*), no Burnett-order correction exists for q_x owing to symmetry constraints in both dilute (Sela & Goldhirsch 1998) and dense (I. Goldhirsch, personal communication 2006) systems. Thus, the large errors in heat flux appear to stem from effects which are super-Burnett-order (third-order in gradients) or larger, as symmetry arguments do not rule out the possibility of super-Burnett contributions to the heat flux (I. Goldhirsch, personal communication 2006). Finally, also shown in figure 10 are the Garzó & Dufty (1999) predictions for heat flux with only the ∇T driving force (line with diamonds); in other words, the ∇n term in the heat flux equation is omitted (see table 1). These results indicate that the main difference in the predictions obtained using the Jenkins (1998) and Garzó & Dufty (1999) theories can be traced to the ∇n term, though these differences are fairly small relative to the overall error in heat flux.

Further support for the non-negligible role of higher-order effects in this system can be gleaned from the work of Santos, Garzó & Dufty (2004), who developed an expression for the heat flux which includes non-Newtonian (higher-order) effects. Their expression is based on a model kinetic equation of the Boltzmann equation and targeted specifically at the bounded conduction problem, though their results are limited to the quasi-elastic and dilute limits. Since, as discussed above, the collisional contributions to the constitutive quantities are not negligible for the range of particle

concentrations explored in this work, a direct comparison between the Santos *et al.* (2004) predictions for heat flux and the MD data is not included here. Nonetheless, it is worth noting that Santos *et al.* (2004) predicts a heat flux which is larger in magnitude than its Navier–Stokes-order counterpart. In the context of figure 10, an increase in heat flux would shift the profiles upward, which is required for a reduction in error. (Recall that the percentage error is defined as $100 \times (\text{theory} - \text{MD})/\text{MD}$, in which a negative value implies that the theory is underpredicting the magnitude of the heat flux.)

Collectively, the results obtained here highlight the unique characteristics of dissipative (inelastic) systems relative to their molecular counterparts. First, for hard-sphere molecular gases, the Dufour contribution to the heat flux is non-existent. Its origin in granular systems stems directly from their dissipative nature. Specifically, consider a system which is initially uniform in temperature and non-uniform in concentration. A corresponding non-uniformity in collision frequency will lead to an uneven distribution of energy loss across the domain, thereby giving rise to a gradient in temperature. The same is not true of molecular systems, since their collisions do not result in energy loss. Secondly, for a bounded conduction problem in which the two bounding walls are of different temperature, a Burnett-order treatment has been found to work well for molecular systems with an effective Kn up to 0.1 (Mackowski *et al.* 1999). Furthermore, previous studies for molecular gases have shown that deviations from Fourier's law are quite small even in the presence of large thermal gradients (Ciccotti & Tenebaum 1980; Mareschal *et al.* 1987; Clause & Mareschal 1988; Santos & Garzó 1995). Thus, the importance of super-Burnett-order contributions (or larger) to the heat flux appears to be a distinctive feature of dissipative systems, at least for the system considered in this work.

5. Concluding remarks

A comparison of the constitutive quantities (γ, $\boldsymbol{\sigma}$ and $\boldsymbol{q}$) extracted from MD simulations and those predicted by Navier–Stokes-order theories indicate the non-negligible role of higher-order effects in the bounded conduction problem studied here. This conclusion is supported by three observations: (i) the relative performance of two Navier–Stokes-order theories for γ at various e is inconsistent with expectations in the bounded conduction problem but consistent with expectations in a gradient-free system (HCS), (ii) an anisotropy in stress components is observed in the bulk region, and (iii) corrections from a Burnett-order theory for dilute, nearly elastic systems provide qualitative improvement to the Navier–Stokes-order predictions. Several further observations related to the heat flux are noteworthy. First, the error of the Navier–Stokes-order predictions for q_x are about one order of magnitude greater than those of γ and P. Secondly, because no Burnett-order corrections exist for q_x (unlike γ and $\boldsymbol{\sigma}$), the higher-order effects must be at least of super-Burnett (third) order. Finally, these higher-order contributions to the heat flux appear to play a more important role than the Dufour contribution (the Navier–Stokes order contribution arising from ∇n).

It is worth pointing out that other causes for the observed mismatch between MD simulations and Navier–Stokes-order predictions are possible, though not likely. First, the theories considered in this work (Jenkins 1998; Garzó & Dufty 1999) employ the lowest non-zero order of a Sonine polynomial expansion for evaluation of collision integrals. Several previous investigations have indicated that additional terms in the expansion may become important only at higher dissipation levels, namely $e \sim <0.7$ (Garzó & Montanero 2002; Brey & Ruiz-Montero 2004; Brey *et al.* 2005), and such

contributions have been confirmed by (Montanero, Santos & Garzó 2007; Noskowicz *et al.* 2007) using two different approaches to derive transport coefficients that go beyond the lowest Sonine truncation. Because the systems forming the basis of the current work are characterized by $e = 0.8$ and 0.99 (these systems are not highly dissipative), however, additional terms in the Sonine expansion are not expected to play a role. Secondly, the Enksog equation itself is known to suffer inaccuracies at high particle concentrations owing to the presence of ring collisions, though such collisions are not expected to play a role at the moderate concentrations considered here ($\nu < 0.1$). A third possibility is the effects induced by the boundaries beyond the nominal Knudsen layers (as are demarcated by the vertical lines in figures 2 to 6 and 8 to 11). For the systems considered in this work, such effects are not likely since the errors observed in the bulk are often the largest at the centre of the domain (furthest from the boundaries). In addition, boundary effects are expected to be small in the bulk, whereas the errors in the heat flux are quite large (up to 40% in magnitude). A fourth possibility is the presence of clusters. As detailed in § 4, however, careful checks were made to ensure that the systems from which the MD data were collected were free of clusters. Finally, it is possible that we have to consider the non-local rheological or liquid-like effects (see, for example, MiDi 2004; Silbert *et al.* 2007). However, such effects are generally associated with dense systems near the transition to solid-like behaviour and as such is unlikely to be a contributing factor in the failings of the Navier–Stokes-order description revealed in this work.

The results obtained in this work give rise to two further questions. First, do higher-order effects contribute in a non-negligible way to the bulk interior of other systems? Higher-order effects also have been noted in simple shear flow (Santos *et al.* 2004), though other systems have not been probed in a similar manner. If higher-order effects are found to be important beyond these two systems, additional theoretical work is required in order to predict such flows. Specifically, the majority of theories developed for granular systems to date are of Navier–Stokes order; only a relatively small number of theories have been developed which incorporate higher-order effects (Kumaran 1997, 2005; Cordero & Risso 1998; Sela & Goldhirsch 1998; Risso & Cordero 2002; Santos *et al.* 2004), and these are restricted to a limited class of systems (e.g. dilute sheared flow).

The second question stemming from this work is: can the importance of higher-order effects in a given granular system be assessed *a priori*? The answer is important not only for those interested in predicting the hydrodynamic profiles occurring in an experimental or simulated system, but also for those interested in extracting constitutive quantities from MD simulations. As mentioned in § 1, such extraction provides a test bed for hydrodynamic descriptions, but it is only reliable if the correct form of the constitutive relation is known beforehand. For example, the HCS is an ideal test bed for Navier–Stokes-order γ since it is a zero-gradient system, whereas systems that can be used for the extraction of Navier–Stokes-order transport coefficients (k, μ, etc.) are not as obvious since non-zero gradients are required to obtain these quantities. If higher-order effects are present in such systems, they cannot easily be separated out as is required for a direct determination of k, μ etc. Furthermore, the importance of accurate extraction of transport coefficients goes beyond its use as a testing ground for existing theories. For example, practical systems include differences in particle shape; a kinetic-theory-based approach for such systems appears intractable at present. Thus, the extraction of transport coefficients from MD provides a much needed alternative for complex systems, assuming that the issues related to higher-order effects can be worked out.

Finally, a few comments on normal stress differences are warranted. In general, such anisotropy can be induced by the boundaries or can arise from Burnett-order effects (Goldhirsch & Sela 1996). An example of the former is a vibro-fluidized bed in which the largest random velocity component at the vibrating base occurs in the direction of vibration (Wildman, Huntley & Parker 2001). Examples of the latter include a simple shear system (Walton & Braun 1986; Jenkins & Richman 1988; Goldhirsch & Sela 1996; Alam & Luding 2003) and the bounded conduction system considered here. In both of the latter systems, the anisotropy can be described by Burnett-order gradients in the flow-field variables, namely those associated with the velocity gradient for the case of simple shear flow (in which $\nabla n = \nabla T = 0$) and those associated with temperature and concentration gradients for the bounded conduction system (in which $\nabla \boldsymbol{V} = 0$, since the average velocity $\boldsymbol{V}$ is zero). In practice, anisotropy may result from a mixture of gradient-induced anisotropy and boundary-induced anisotropy, as is the case for the vibro-fludized bed. However, the normal stress differences arising from particle–wall interactions are expected to attenuate once the particles have engaged in enough particle–particle collisions. Specifically, on length scales greater than the thickness of the Knudsen layer (Galvin *et al.* 2007), anisotropy driven by the boundary is effectively eliminated, and any remaining anisotropy in the bulk region is driven by gradients of Burnett order or greater. As mentioned above, the occurrence of such anistropic effects in the bulk region suggests the need for higher-order theories. Similarly, the presence of such effects in the boundary region calls for improved 'apparent' boundary conditions, analogous to those use to described rarefied gases.

The authors would like to thank Isaac Goldhirsch for conversations on this topic. The authors are grateful for the funding support provided by the Engineering and Physical Sciences Research Council through Grants EP/D030676/1 and GR/R75694/01. J. E. G. and C. M. H. would also like to express their gratitude to the National Science Foundation for additional support via an international supplement to Grant CTS-0318999. J. E. G. is also thankful for partial stipend support provided by the Minority Mentoring Internship Program at the Department of Energy National Energy Technology Laboratory. C. M. H. and R. D. W. would also like to acknowledge those involved with the Granular Physics Workshop at the Kavli Institute of Theoretical Physics (supported in part by the National Science Foundation under grant number PHY99-07949), which was an impetus for much of this work.

REFERENCES

Alam, M. & Luding, S. 2003 Rheology of bidisperse granular mixtures via event-driven simulations. *J. Fluid Mech.* **476**, 69.

Brey, J. J. & Ruiz-Montero, M. J. 2004 Simulation study of the Green–Kubo relations for dilute granular gases. *Phys. Rev.* E **70**, 051301.

Brey, J. J., Dufty, J. W., Kim, C. S. & Santos, A. 1998 Hydrodynamics for granular flow at low density. *Phys. Rev.* E **58**, 4638.

Brey, J. J., Ruiz-Montero, M. J. & Moreno, F. 2001 Hydrodynamics of an open vibrated system. *Phys. Rev.* E **63**, 061305.

Brey, J. J., Ruiz-Montero, M. J., Maynar, P. & Garcia de Soria, M. I. 2005 Hydrodynamic modes, Green-Kubo relations, and velocity correlations in dilute granular gases. *J. Phys. Cond. Matter* **17**, S2489.

Brey, J. J., Dominguez, A., Garcia de Soria, M. I. & Maynar, P. 2006 Mesoscopic theory of critical fluctuations in isolated granular gases. *Phys. Rev. Lett.* **96**, 158002.

Brilliantov, N. V. & Pöschel, T. 2004 *Kinetic Theory of Granular Gases*. Oxford University Press.

Campbell, C. S. 1990 Rapid granular flows. *Annu. Rev. Fluid Mech.* **22**, 57.

Campbell, C. S. & Gong, A. 1986 The stress tensor in a two-dimensional granular shear flow. *J. Fluid Mech.* **164**, 107.

Carnahan, N. F. & Starling, K. E. 1969 Equation of state of non-attracting rigid spheres. *J. Chem. Phys.* **51**, 635.

Cercignani, C. 1987 *The Boltzmann Equation and its Applications*. Springer.

Ciccotti, G. & Tenebaum, A. 1980 Canonical ensemble and nonequilibrium states by molecular dynamics. *J. Stat. Phys.* **23**, 767.

Clause, P. J. & Mareschal, M. 1988 Heat-transfer in a gas between parallel plates – moment method and molecular-dynamics. *Phys. Rev.* A **38**, 4241.

Cordero, P. & Risso, D. 1998 Nonlinear transport laws for low density fluids. *Physica* A **257**, 36.

Curtis, J. S. & van Wachem, B. 2004 Modeling particle-laden flows: a research outlook. *AIChE J.* **50**, 2638.

Dahl, S. R. & Hrenya, C. M. 2004 Size segregation in rapid, granular flows with continuous size distributions. *Phys. Fluids* **16**, 1.

Ferziger, J. H. & Kaper, H. G. 1972 *Mathematical Theory of Transport Processes in Gases*. Elsevier.

Galvin, J. E., Dahl, S. R. & Hrenya, C. M. 2005 On the role of non-equipartition in the dynamics of rapidly flowing granular mixtures. *J. Fluid Mech.* **528**, 207.

Galvin, J. E., Hrenya, C. M. & Wildman, R. D. 2007 On the role of the Knudsen layer in rapid granular flows. *J. Fluid Mech.* **585**, 73.

Garzó, V. & Dufty, J. 1999 Dense fluid transport for inelastic hard spheres. *Phys. Rev.* E **59**, 5895.

Garzó, V. & Montanero, J. M. 2002 Transport coefficients of a heated granular gas. *Physica* A **313**, 336.

Goldhirsch, I. 2003 Rapid granular flows. *Annu. Rev. Fluid Mech.* **35**, 267.

Goldhirsch, I. & Sela, N. 1996 Origin of normal stress differences in rapid granular flows. *Phys. Rev.* E **54**, 4458.

Goldhirsch, I. & Zanetti, G. 1993 Clustering instability in dissipative gases. *Phys. Rev. Lett.* **70**, 1619.

Goldhirsch, I., Noskowicz, S. H. & Bar-Lev, O. 2004 Theory of granular gases: some recent results and some open problems. *J. Phys. Cond. Matter* **17**, 2591.

Haff, P. K. 1983 Grain flow as a fluid-mechanical problem. *J. Fluid Mech.* **134**, 401.

Herbst, O., Müller, P., Otto, M. & Zippelius, A. 2004 Local equation of state and velocity distributions of a driven granular gas. *Phys. Rev.* E **70**, 051313.

Herbst, O., Müller, P. & Zippelius, A. 2005 Local heat flux and energy loss in a two-dimensional vibrated granular gas. *Phys. Rev.* E **72**, 141303.

Hopkins, M. & Louge, M. 1991 Inelastic microstructure in rapid granular flows of smooth disks. *Phys. Fluids* A **3**, 47.

Jenkins, J. T. 1998 Kinetic theory for nearly elastic spheres. In *Physics of Dry Granular Media* (ed. H. J. Hermann, J. P. Hovi & S. Luding). Kluwer.

Jenkins, J. T. & Richman, M. W. 1988 Plane simple shear of smooth inelastic circular disks: the anisotropy of the second moment in dilute and dense limits. *J. Fluid Mech.* **192**, 313.

Kumaran, V. 1997 Velocity distribution function for a dilute granular material in shear flow. *J. Fluid Mech.* **340**, 319.

Kumaran, V. 2005 Kinetic model for sheared granular flows in the high Knudsen number limit. *Phys. Rev. Lett.* **95**, 108001.

Lasinski, M. E., Curtis, J. S. & Pekny, J. F. 2004 Effect of system size on particle-phase stress and microstructure formation. *Phys. Fluids* **16**, 265.

Liss, E. D. & Glasser, B. J. 2001 The influence of clusters on the stress in a sheared granular material. *Powder Technol.* **116**, 116.

Mackowski, D., Papadopoulos, D. H. & Rosner, D. E. 1999 Comparison of Burnett and DSMC predictions of pressure distributions and normal stress in one-dimensional, strongly nonisothermal gases. *Phys. Fluids* **11**, 2108.

Mareschal, M., Kestemont, E., Baras, F., Clementi, E. & Nicolis, G. 1987 Nonequilibrium states by molecular-dynamics – transport-coefficients in constrained fluids. *Phys. Rev.* A **35**, 3883.

Martin, T. W., Huntley, J. M. & Wildman, R. D. 2006 Hydrodynamic model for a vibrofluidized granular bed. *J. Fluid Mech.* **535**, 325.

MiDi, G. D. R. 2004 On dense granular flows. *Eur. Phys. J.* E **14**, 341.

Montanero, J. M., Santos, A. & Garzó, V. 2007 First-order Chapman–Enskog velocity distribution function in a granular gas. *Physica* A **376**, 75.

Noskowicz, S. H., Bar-Lev, O., Serero, D. & Goldhirsch, I. 2007 Computer-aided kinetic theory and granular gases. *Europhys. Lett.* **79**, 60001.

Pöschel, T. & Schwager, T. 2005 *Computational Granular Dynamics*. Springer.

Press, W. H., Flannery, B. P., Teukolsky, S. A. & Vetterling, W. T. 1992 *Numerical Recipes in C: The Art of Scientific Computing*. Cambridge University Press.

Risso, D. & Cordero, P. 2002 Dynamics of rarefied gases. *Phys. Rev.* E **65**, 021304.

Santos, A. & Garzó, V. 1995 In *Rarefied Gas Dynamics 19* (ed. J. Harvey & G. Lord). Oxford University Press.

Santos, A., Garzó, V. & Dufty, J. 2004 Inherent rheology of a granular fluid in uniform shear flow. *Phys. Rev.* E 061303.

Sela, N. & Goldhirsch, I. 1998 Hydrodynamic equations for rapid flows of smooth inelastic spheres, to Burnett order. *J. Fluid Mech.* **361**, 41.

Shattuck, M. D., Bizon, C., Swift, J. B. & Swinney, H. L. 1999 Computational test of kinetic theory of granular media. *Physica* A **274**, 158.

Silbert, L. E., Grest, G. S., Brewster, R. & Levine, A. J. 2007 Rheology and contact lifetimes in dense granular flows. *Phys. Rev. Lett.* **99**, 068002.

Soto, R., Mareschal, M. & Risso, D. 1999 Departure from Fourier's law for fluidized granular media. *Phys. Rev. Lett.* **83**, 5003.

Sundaresan, S. 2000 Perspective: Modeling the hydrodynamics of multiphase flow reactors: Current status and challenges. *AIChE J.* **46**, 1102.

Sunthar, P. & Kumaran, V. 2001 Characterization of the stationary states of a dilute vibrofluidized granular bed. *Phys. Rev.* E **64**, 041303.

Tan, M.-L. & Goldhirsch, I. 1997 Intercluster interactions in rapid granular shear flows. *Phys. Fluids* **9**, 856.

Walton, O. R. & Braun, R. L. 1986 Stress calculations for assemblies of inelastic spheres in uniform shear. *Acta Mech.* **63**, 73.

Wassgren, C. & Curtis, J. S. 2006 The application of computational modeling to pharmaceutical materials science. *MRS Bull.* **31**, 900.

Wildman, R. D., Huntley, J. M. & Parker, D. J. 2001 Granular temperature profiles in three-dimensional vibrofludized granular beds. *Phys. Rev.* E **63**, 061311.